Plasma Sci. Technol. **24** (2022) 124021 (18pp) https://doi.org/10.1088/2058-6272/acaa8d

Towards advanced divertor configurations on the J-TEXT tokamak

Yunfeng LIANG (梁云峰)[1,2,3], **Zhipeng CHEN** (陈志鹏)[1], **Nengchao WANG** (王能超)[1], **Zhifeng CHENG** (程芝峰)[1], **Alexander KNIEPS**[2], **Song ZHOU** (周松)[1], **Bo RAO** (饶波)[1], **Shuai XU** (徐帅)[2], **Philipp DREWS**[2], **Xiaolong ZHANG** (张晓龙)[4], **Hao WANG** (王灏)[1], **Zhaosu WANG** (王昭苏)[1], **Jie YANG** (阳杰)[1,2], **Xin XU** (徐鑫)[1], **Jiankun HUA** (华建坤)[1,2], **Qinghu YANG** (杨庆虎)[1], **Wei YAN** (严伟)[1], **Cunkai LI** (李存凯)[1], **Yutong YANG** (杨雨桐)[1], **Shuhao LI** (李述豪)[1], **Shaocheng LIU** (刘少承)[3], **Lin NIE** (聂林)[4], **Ting LONG** (龙婷)[4], **Liang LIAO** (廖亮)[2,3], **Fuqiong WANG** (王福琼)[5], **Yasuhiro SUZUKI**[1,6] **and the J-TEXT Team**[1]

[1] International Joint Research Laboratory of Magnetic Confinement Fusion and Plasma Physics, State Key Laboratory of Advanced Electromagnetic Engineering and Technology, School of Electrical and Electronic Engineering, Huazhong University of Science and Technology, Wuhan 430074, People's Republic of China
[2] Forschungszentrum Jülich GmbH, Institut für Energie- und Klimaforschung—Plasmaphysik, Partner of the Trilateral Euregio Cluster (TEC), Jülich 52425, Germany
[3] Institute of Plasma Physics, Chinese Academy of Sciences, Hefei 230031, People's Republic of China
[4] Southwestern Institute of Physics, Chengdu 610041, People's Republic of China
[5] Department of Applied Physics, College of Science, Donghua University, Shanghai 201620, People's Republic of China
[6] Graduate School of Advanced Science and Engineering, Hiroshima University, Higashi-Hiroshima 739-8527, Japan

E-mail: y.liang@fz-juelich.de

Received 24 October 2022, revised 9 December 2022
Accepted for publication 9 December 2022
Published 30 December 2022

Abstract

Developing advanced magnetic divertor configurations to address the coupling of heat and particle exhaust with impurity control is one of the major challenges currently constraining the further development of fusion research. It has therefore become the focus of extensive attention in recent years. In J-TEXT, several new divertor configurations, including the high-field-side single-null poloidal divertor and the island divertor, as well as their associated fundamental edge divertor plasma physics, have recently been investigated. The purpose of this paper is to briefly summarize the latest progress and achievements in this relevant research field on J-TEXT from the past few years.

Keywords: divertor, tokamak, magnetically confined fusion

(Some figures may appear in colour only in the online journal)

1. Introduction

1.1. State of the art of fusion energy research

Since the beginning of the 21st century, fusion research has entered a research era focusing on long-pulse steady-state high-performance integrated scenario development. Several large superconducting fusion devices, such as LHD [1] in Japan, EAST [2] in China, KSTAR [3] in Korea, W7-X [4] in Germany, and WEST [5] in France, have been put into operation one after another. However, the results from these experiments suggest that overheating of the target plate and impurity accumulation in the plasma core tend to occur once the operating domain is extended to the high-power long-pulse steady-state H-mode plasma regime, especially when

using an ITER-like tungsten divertor and metallic plasma-facing components (PFCs) [6]. Today, we recognize more clearly than ever that the coupling of heat and particle exhaust with impurity control is one of the most difficult bottlenecks restricting further development of fusion research, and this problem has therefore become the focus of extensive attention in recent years.

1.2. Divertor physics and challenges

The standard poloidal divertor, characterized by a single magnetic field null (X-point) located in the divertor region and two poloidal legs intersecting with the divertor at the strike points, has been developed on many devices to handle power and particle/impurity exhaust, and has enabled significant progress in tokamak physics studies [7]. Four critical divertor physics issues, which include (i) power exhaust; (ii) D/T and He pumping; (iii) reduction of impurity production (source); and (iv) impurity screening by the divertor scrape-off layer (SOL), have been identified and well investigated. Although the standard poloidal divertor configuration has been planned for ITER, it has been recognized that this concept might be problematic for the high-performance era of ITER operation, and could be inappropriate for a future reactor.

For a conduction-dominated SOL, the basic scaling of the power decay length, λ_q, is given by

$$\lambda_q \approx \pi q R \sqrt{\frac{\chi_\perp}{\chi_\parallel}}; \tag{1}$$

here, q is the edge safety factor, which is inversely proportional to the plasma toroidal current, I_p, or the strength of the poloidal magnetic field, B_θ. R is the major radius of the plasma. $\chi_\parallel$ and $\chi_\perp$ are the thermal diffusion coefficients in the directions parallel and perpendicular to the field lines, respectively. The first three items on the right-hand side of equation (1) approximately represent the field-line connection length, $L_\parallel$, in the SOL, which is determined by the magnetic configuration and the structure of the divertor target plate.

Due to the significant anisotropic transport effects inside magnetized hot plasmas, where the plasma transport along the field lines is several orders of magnitude higher than the cross-field transport, the plasma parameter profiles decay rapidly inside the SOL, which causes a thin power decay length. For ITER and future fusion reactors, there will be a heat flow of the order of 100 megawatts from the plasma core into the SOL, and most of the heat will be exhausted through the divertor. The λ_q for ITER predicted based on empirical scalings is only about 1 mm, resulting in a serious peak value of about 50 MW m^{-2} for the steady-state heat load, far exceeding the limit of existing materials ($\sim$10 MW m^{-2}) [8]. Therefore, to sustain the steady-state high-performance burning plasma operation in a future fusion reactor, it is of great significance to both increase the power deposition area of the divertor plate and reduce the thermal load power flowing to the target plate at the same time. In order to meet this challenge, the following key aspects related to fundamental physics research on the advanced divertor configuration have to be carried out:

- ***Magnetic topology***. By optimizing the magnetic configuration and the structure of the target plate, the magnetic field lines in the SOL are expanded or lengthened, thereby increasing the deposition area of the thermal load on the target plate.
- ***Plasma transport***. There is a need to increase the effective radial transport of heat and particles and reduce the peak heat load of the target plate; the divertor and the SOL plasma transport physics should be explored, and the impurity screening effect should be further optimized.
- ***Heat load dissipation***. By seeding impurities at the plasma boundary or increasing the plasma density, the total exhaust power, including alpha particle heating and external heating power, should be dissipated as much as possible before being transmitted from the core to the wall, so that the temperature of the first wall can be controlled at a safe level.

In principle, these three issues are interconnected with each other. For a standard poloidal X-point divertor plasma, assuming that the total conductive power flowing into the SOL is balanced by volumetric losses, a simple zero-order detachment criterion [7] can be defined as

$$\frac{14}{3} C_Z L_Z n_\mathrm{u}^2 L_\parallel \approx q_\mathrm{u}, \tag{2}$$

where C_Z is the impurity fraction, L_Z is the plasma radiation efficiency, and q_u is the parallel upstream heat flux. Therefore, increasing the field-line connection length at the SOL will facilitate the expansion of the divertor wetted area, as well as easy access of detachment with lower upstream plasma density, n_u.

1.3. Existing advanced divertor configurations and open questions

In addition, there are still two essential technical challenges that have to be solved:

- Core–edge integration, which develops and demonstrates dissipative/detached divertor solutions for power and particle control sufficient for extrapolation to power plant conditions.
- Power exhaust solutions taking into account both steady-state and transient heat loads.

These tasks have been recognized as much more complicated problems due to the nonlinear coupling of multiple physical processes over a wide range of overlapping spatial and temporal scales for long-pulse high-performance plasma scenario development. Explorations of new divertor configurations as well as long-pulse demonstrations of sustained high-performance plasma operation with integration of the optimized core–edge coupling and power exhaust solutions have been carried out in many stellarator and tokamak devices [6, 9–13].

In stellarators, both the helical divertor on LHD [14] and the island divertors [15] on W7-AS and W7-X, featuring a three-dimensional (3D) edge magnetic configuration and longer field-line connection lengths at the SOL (in the

magnitude of 10^2–10^3 m, much longer than the electron mean free path), have demonstrated excellent performances in obtaining either stable strongly radiating divertor plasmas or steady-state full detachment. During the first W7-X high-performance experimental campaign OP1.2, full divertor power detachment was established and sustained stably. Furthermore, a new record of the triple product of 6.4×10^{19} keV s m^{-3} for stellarator plasmas was achieved with pellet injections in a standard island divertor configuration on W7-X. These results demonstrated good core–edge integration properties of the island divertor concept for stellarator plasma operation.

Recently, a new resilient divertor concept, the so-called non-resonant divertor [16], was designed for advanced stellarators optimized for reduced neoclassical transport. A feature of this divertor concept is that the locations of the strike points on divertor targets are not strongly affected as the plasma configuration varies (for example, due to the inclusion of plasma current).

In tokamaks, two major categories of two-dimensional (2D) advanced poloidal divertor configurations have been developed, including

- High-order null divertors, such as the snowflake and the cloverleaf divertors.
- High-flux expansion and long poloidal leg divertors with multiple X-points, such as the Super-X divertor and the X-point target divertor.

The geometric features of the 2D advanced poloidal divertor configurations and their profound impacts to improve certain detachment characteristics have been recently validated by experiments and modeling on TCV [17], DIII-D [18], and EAST [19]. The experimental observations show more complicated edge transport mechanisms eclipsing the edge impurity transport analysis using 2D fluid models, and raise many open questions on the fundamental physics of divertor plasmas, such as neoclassical drift effects and their impact on the upstream profiles, inner–outer/up–down divertor balance and divertor power decay length and detachment. On the long-legged and Super-X divertor configurations [20], the upcoming MAST Upgrade experiment will provide critical data not only on the physics but also on the engineering performance. However, none of these 2D advanced poloidal divertor concepts can decouple the significant inverse relationship between the plasma toroidal current and the divertor power decay length.

The dynamic ergodic divertor (DED) concept [11, 12], characterized by the formation of a proper 3D edge ergodic zone, an area of open magnetic field lines, a laminar zone, and a tangle structure at the plasma boundary, has been introduced in the TEXTOR tokamak plasma by applying helical magnetic field perturbations resonating at the $q = 3$ rational magnetic flux surface. The toroidal symmetry of the edge plasma profiles, as well as the heat and particle flux distributions on the divertor target plate, were found to be broken. A prominent feature of the ergodic divertor is its ability to control the edge plasma transport, as well as to mitigate/suppress transient heat loads caused by the edge plasma instability, such as edge-localized modes (ELMs) in H-mode plasmas [21–26].

It is foreseen that more and more upcoming new experiments and devices will contribute to the development of advanced magnetic divertor configurations, such as HL-2M [27] and DTT [28]. These experiments should enable the development of an integrated divertor solution that can be based on one of the reviewed magnetic configurations, advanced target technologies, and compatibility with the core plasma requirements.

1.4. The J-TEXT tokamak

The Joint-Texas Experimental tokamak (J-TEXT) [29], formerly known as TEXT/TEXT-U [30], was moved from the University of Texas in Austin to Huazhong University of Science and Technology in 2004. It is a conventional middle-sized tokamak with a major radius $R_0 = 1.05$ m, minor radius $a = 25$–29 cm, and a toroidal magnetic field, B_t, of up to 3.0 T. Since it resumed operation in 2007, a set of new saddle coils including 24 (3×8) in-vessel and 6 external coils has been installed for flexible adjustment of resonant magnetic perturbations (RMPs) [31]. Furthermore, a 105 GHz electron cyclotron resonant heating system (ECRH) with a maximal power of 500 kW has been applied for electron-dominated heating [32].

At present, J-TEXT is capable of operating in a variety of plasma configurations, including limiter, single- (top, middle, or bottom) or double-null high-field-side (HFS) divertor, and island divertor [33]. As part of a long-term fusion research roadmap in China, the J-TEXT experimental program aims to develop fundamental physics and control mechanisms of high-temperature tokamak plasma confinement and stability in support of the successful operation of ITER and the design of future fusion reactors, such as CFETR [34].

1.5. This paper

In the past five years, a great effort from the J-TEXT team has been oriented towards advanced divertor configurations, and their related fundamental edge divertor plasma physics. The following subtopics have been pursued and will be continued.

- Realize and characterize HFS poloidal divertor plasmas on J-TEXT with a reliable plasma shape and stability control mechanism, and study the fundamental physics of the density limit, impurity transport, radiating divertor, detachment, and the impact of E_r on the up–down asymmetry of divertor loads.
- Develop and optimize the island divertor configuration for a tokamak plasma, considering the stability of the edge islands, impurity screening effects, and 3D divertor heat loads.
- Investigate new divertor concepts, such as the formation of a stochastization boundary with either 3D non-axisymmetric SOL current filaments induced by electrode biasing, or with 3D RMP coils in a limiter or HFS poloidal divertor configuration.

- Develop and evaluate modern edge plasma diagnostics, measuring the edge turbulence and turbulent transport, upstream and downstream plasma profiles, and 2D distributions of divertor impurities, plasma flow, and radiation.
- Establish and validate an integrated simulation package to calculate plasma magnetohydrodynamic (MHD) equilibrium, edge particle/impurity transport and stability, and divertor heat flux distributions, in order to support HFS divertor experiments, which can also properly support island divertor investigations, in which the edge dynamics are dominated by 3D fields.

In this overview paper, the advanced progress and results towards advanced divertor configurations achieved on the J-TEXT tokamak over the last five years, especially on the above subtopics, will be presented.

2. Developments of edge, SOL, and divertor plasma diagnostics

Various edge diagnostics have been developed to study the edge plasma parameters in the past decade, which support the achievement of advanced divertor configuration studies on J-TEXT by obtaining information on the edge plasma behavior [35–44]. In this section, a review of these diagnostics, including reciprocating probes, limiter probes, visible imaging systems, and visible spectroscopic diagnostics, is given. An overview of the presented diagnostics is shown in figure 1. These diagnostics are dedicated to measuring the edge turbulence and turbulent transport, upstream and downstream plasma parameters, and edge plasma flows and impurity distributions. The diagnostics with their respective measurement roles are listed in table 1.

2.1. Reciprocating probes

Two sets of reciprocating manipulators are installed at the top windows of two different toroidal positions, port #12 and port #13. These manipulators have a maximum plunge length of 5 cm with a typical speed of about 1 m s^{-1}. Several types of probe heads that are compatible with the manipulators are developed to measure the local plasma parameters at the edge region.

2.1.1. Langmuir magnetic probe. The Langmuir probe is commonly applied in tokamak devices [35]. Its configuration was also initially developed on J-TEXT, providing data on the electron density and temperature, the floating potential, and fluctuations of these quantities in the boundary region with a temporal resolution of 0.5 μs.

A magnetic probe array was developed to measure the local magnetic fluctuations at the plasma edge [36]. This magnetic probe array consists of four 2D magnetic probes, detecting local poloidal and radial magnetic fields at the plasma edge within the last closed flux surface (LCFS).

Finally, this probe was updated with a composition of Langmuir and magnetic probes, named the 'combined Langmuir magnetic probe' [37]. As shown in figure 1, the Langmuir probe is ceramic on the top, with eight graphite probe pins distributed in two stages. Stage #2 is 3 mm higher than stage #1, so that the probe pins on different stages can obtain electrostatic signals at different radial positions. The middle ceramic holds the 3D magnetic probe, which is made of enameled copper wire with an outer diameter of 0.23 mm wound on the middle ceramic skeleton. Specific cuts are embedded into the graphite sleeve to minimize the impact of eddy currents.

2.1.2. Retarding field analyzer (RFA). The ion energy transport in the SOL is of importance in understanding the plasma–surface interaction [38]. To directly measure the ion temperature, a bidirectional RFA is employed on J-TEXT. The RFA array (the slit plate, two grids, and collector) is aligned along the magnetic field. The basic RFA and the eiRFA (for electron and ion temperature measurement) schemes were implemented in succession [39]. For the RFA scheme, the ion temperature could be evaluated by sweeping the collector voltage and current matching Maxwellian distribution. The eiRFA scheme consists of the single-probe principle and RFA principle, which is achieved by adding an AC biased voltage on the slit plate to scan the SP-I-V (slit plate acting as single probe), as well as to sift the ions into the eiRFA. Thus, the electron temperature and ion temperature can be evaluated by the eiRFA simultaneously.

2.2. Limiter probes

The limiter target electrostatic measurement system, including limiter grounding current sensors and Langmuir probes, was newly developed for the measurement of the limiter target area [40]. Additionally, a limiter Langmuir probe array (LLPA) embedded in graphite tiles of limiters was also built for a more localized measurement. The LLPA consists of 54 graphite probes, which are arranged symmetrically with respect to the mid-plane. The probes are distributed in 8 mm spaced pairs, with the distance between two adjacent pairs being 25 mm. This dense distribution at the HFS is beneficial for investigating the electrostatic parameters of the HFS divertor X-point. Besides the different poloidal positions, the radial position of the probe tip relative to the LCFS is also different. A coaxial line transmits the signal to the data acquisition system in a nearby isolated cabinet through the sampling circuit. The sampling rate of a single acquisition channel is up to 750 kHz.

2.3. Non-invasive diagnostics

2.3.1. Visible light high-speed imaging system. A visible light high-speed imaging system (VLHIS) was installed on the J-TEXT tokamak to measure the spatial distribution of visible light in the vacuum chamber [41]. This system views the plasma tangentially from an outer port at the height of the vacuum vessel's mid-plane. In order to capture the plasma

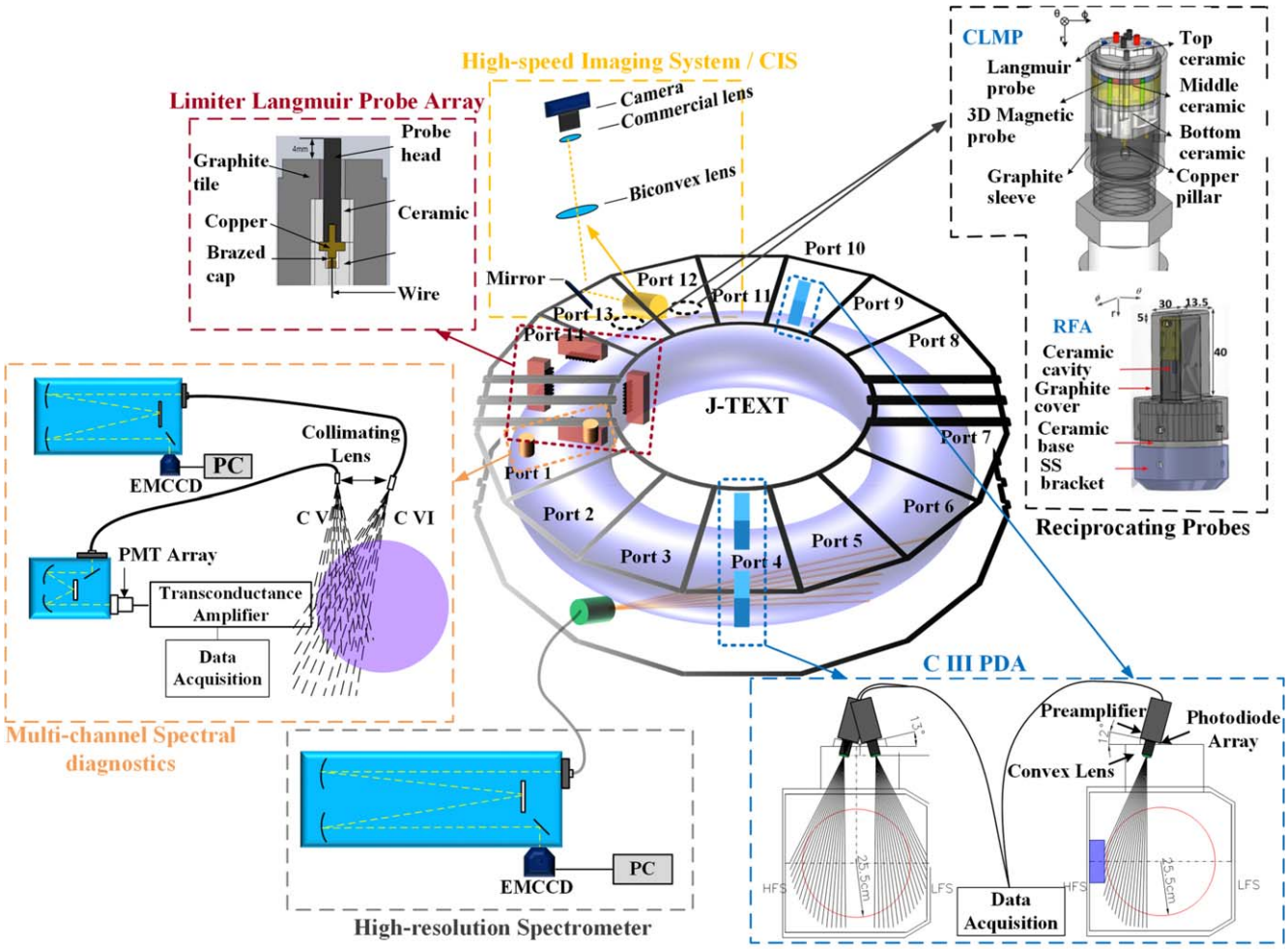

Figure 1. Layout of edge plasma diagnostics on J-TEXT.

Table 1. Roles of developed edge plasma diagnostics.

Diagnostic		Function
Reciprocating probes	Langmuir probe	Upstream n_e, T_e, V_f, and their fluctuations
	Magnetic probe	Upstream B fluctuations
	Retarding field analyzer	T_i
Limiter probes	Downstream n_e, T_e, V_f, and their fluctuations	
High-speed imaging system	Visible image	
Spectral diagnostics	C III photodiode array	C III distribution
	High-resolution spectrometer	C III and C V flows
	Multi-channel spectral diagnostic	$n_{C\ V}$ and $n_{C\ VI}$ distribution
	Doppler coherence imaging spectroscopy	$I_{C\ III}$ image, $V_{C\ III}$ image

images of the whole poloidal cross-section of the vacuum vessel, the camera system is mounted at a tangential window on the mid-plane of the vacuum vessel, looking clockwise. A customized optical system was designed to move the CCD camera away from the window, avoiding disturbances on the camera caused by the strong toroidal magnetic field. This optical system includes four components, two biconvex lenses, a commercial lens, and a reflector. One biconvex lens 1 ($f = 80$ mm) is placed close to the tangential window to increase the field of view because the tangential window could occlude some light from the low-field side (LFS) or the HFS.

2.3.2. High-resolution ultraviolet/visible spectrometer. A high-resolution ultraviolet/visible spectroscopic system was developed to measure the rotation velocity of light impurities in the edge region of J-TEXT [42, 43]. Carbon V (C V 227.09 nm) and carbon III (C III 229.69 nm) were chosen as the lines to be measured. These two lines can be acquired by

the spectrometer together. Therefore the two ions' velocities can be obtained simultaneously.

The spectroscopy system (shown in figure 1) consists of a 1.33 m focal length monochromator with a 1800 g mm^{-1} grating, an electron-multiplying charge-coupled device (EMCCD) camera with 1024 × 1024 pixels, and a fiber optic light collection system with 17 viewing channels. Sixteen of these viewing channels, with each channel consisting of two fibers (diameter = 200 μm), are used for toroidal rotation measurement based on the Doppler shift. The mean diameter of the viewing cones inside the plasma is about 8 mm, which provides the good spatial resolution necessary for rotation velocity measurements. A channel is dedicated to the reference channel giving zero velocity, for which the line of sight is perpendicular to the horizontal plane and passes through the plasma center.

A spatial deconvolution technique is used to obtain the local rotation velocity, since the collected light from the plasma is line-integrated. In this technique, the plasma cross-section is divided into several layers according to the number of viewing channels, and the parameters, including the emission intensity, rotation velocity, and ion temperature, are assumed to be symmetric in the toroidal direction. The plasma parameters of the inner layers are determined by removing the contribution from the outer layers. Hence, the relative differences among the measurement channels in spectral responsibility, wavelength deviation, and instrument function must be known through careful calibration. Here, the bulk plasma is applied as the calibration light source to determine the spectral responsiveness and wavelength deviation.

2.3.3. Spectroscopic diagnostics for edge impurity studies. Several visible/UV spectroscopic diagnostics are composed to form a light impurity diagnostic system, providing several impurity (for carbon ions, specifically) radiation profile measurements in the plasma edge region [44]. It consists of two carbon III (C III 464.7 nm) photodiode arrays (PDAs), one carbon V (C V 227.09 nm) diagnostic, and one carbon VI (C VI 529.26 nm) diagnostic.

The two PDAs are identical. Each is configured with an 18-channel PDA, a specified front C III filter (center wavelength of 466 nm, bandwidth of 5 nm), a collimator, and an in-built amplifier. Two PDAs are installed at port 4, dedicated to measuring the C III emission on the HFS and LFS. The spatial resolution, time resolution, and coverage area of the C III diagnostic are 13 mm, 100 μs, and r_{chord} = 7–29 cm, respectively.

The C V diagnostic was developed to measure the emission profile of C V in the HFS region, shown in the orange area in figure 1. This system consists of a 12-core fiber bundle with a core diameter of 400 μm for light collection, an aberration-corrected monochromator, one photomultiplier tube (PMT) array, and an amplifier. The monochromator, with a focal length of 300 mm, a grating of 1200 g mm^{-1}, and an effective aperture of f/4.2, can be used to select specific wavelengths (usually for C V 227.09 nm). The PMT is used to convert light into current signals, which are then converted to voltage signals via the amplifier. The temporal resolution, spatial resolution, and coverage area of the array are 0.1 ms, 12 mm, and r_{chord} = 25.5 cm to 12 cm, respectively.

The configuration of the C VI diagnostic is similar to the high-resolution ultraviolet/visible spectrometer. It consists of a 10-core fiber bundle with a core diameter of 200 μm for light collection, an aberration-corrected monochromator with a focal length of 750 mm for light dispersion, and an EMCCD camera with 512 × 512 pixels for light detection. The grating is spaced at 1200 g mm^{-1}. The wavelength range is 190–2100 nm, but the central wavelength is set to 529.3 nm to measure the C VI line in common operation. Since the distribution of C VI radiation is relatively wide, an acceptance angle of 30 degrees is applied to achieve an appropriate viewing coverage area to observe the C VI behavior in the HFS region. The temporal resolution is mainly determined by the radiation intensity and is usually set to 10 ms.

2.3.4. Doppler coherence imaging spectroscopy. Doppler coherence imaging spectroscopy (CIS) has been installed on the J-TEXT tokamak to provide the 2D profile of the emissivity and the flow of C III impurity ions via the Doppler shift of their characteristic spectrum [45]. It shares the same window as VLHIS (which is presented in section 2.3.1). The imaging process relies on commercial lenses, achieving the system's focal length of 70 mm. A custom band-pass filter is used to isolate the target spectral line (C III 464.7 nm). The key part of the CIS diagnostic is a static polarization interferometer, which is based on spatial multiplexing techniques with a spatially varied phase delay (along one detector dimension). Adding the Phantom V2012 high-speed camera, the system can reach a temporal resolution of 5 ms. The spatial resolution is determined by the measurement to be provided. For the emissivity measurement, it is up to ~0.8 mm in the 2D space. For the flow measurement, the spatial resolution is ~0.8 mm in the horizontal direction and ~9 mm in the vertical direction due to the limitation of the interference fringes. The emissivity and the flow profiles are evaluated through a specifically developed spatial inversion, based on the Tikhonov method, which was successfully developed and applied to reconstruct the topography of flow on J-TEXT.

2.3.5. Discussion and future challenges. By combining these diagnostics, many physics processes linked to the formation of divertor plasmas could be deduced. The edge plasma temperature and the electron and the edge impurity intensity are used to understand the plasma and wall interactions. The edge electrical field and edge flow could be applied to identify the formation of the X-point. Adding the turbulence information, which is represented by the fluctuations of plasma parameters, the transition of edge plasma transport is involved.

To depict a clearer image assisting the deeper study of the various plasma behaviors in the unique divertor configurations on J-TEXT, the edge diagnostics are kept in

continuous improvement with more measurement channels in development, such as C III PDAs and target probes. The flexibility of the RFA will be expanded to approach the ion temperature measurement for both upstream and downstream plasma, which may show the difference between the electron transport channel and ion transport channel at the edge. To interpret the large data collections provided by these systems, a comprehensive data flow that combines various diagnostics needs to be developed.

3. Integration of numerical simulations for edge and divertor plasma transport

To keep up with the shifting demand from fundamental research into operational scenario development, simulation development in fusion is trending towards integrated modeling approaches, where individual physics codes focusing on a single aspect of plasma physics (MHD equilibrium, instabilities, plasma transport, impurity transport, plasma–wall interaction (PWI), wall evolution) are increasingly employed together to reproduce experimental scenarios and allow the planning of future devices and their operation. This shift has substantially increased the validation burden on the individual physics codes, as validating a single aspect of a multi-stage model can only be done once sufficient trust is established in its other stages.

In the recent years, substantial progress has been made in challenging and improving the accuracy of workhorse codes for integrated scenario applications. In the plasma edge, this primarily requires tying together the individual aspects of edge magnetic field evolution (bootstrap current, MHD equilibrium, MHD instability), main plasma transport, impurity transport and radiation, and PWI, into models for advanced divertor configurations.

The advancements discussed in this section can be roughly categorized into four different areas:

- 3D edge field modeling. In advanced divertor scenarios, accurate prediction of transport and wall interaction requires precise knowledge of the edge magnetic field structure. Here, the application of full 3D equilibrium and instability codes has substantially increased the precision of predicted and reconstructed magnetic topologies.
- 3D transport modeling. RMP-perturbed poloidal divertors and island divertors require transport codes capable of full 3D simulation. In this area, substantial advances were made by integrating codes before they were mainly developed for stellarator application with tokamak scenarios.
- Accurate transport and PWI modeling for advanced divertor configurations. Novel divertor configurations, such as symmetric HFS divertors, snowflake configurations, or the Super-X, are particularly sensitive to drift effects, which are particularly challenging to model correctly. Here, significant progress has been made to employ J-TEXT's HFS divertor (whose inherent up–down symmetry makes it uniquely suitable for drift effect studies) as a benchmarking facility for code validation.
- Active control of unstable magnetic configurations. Tokamak operation regularly requires trading plasma stability against performance. Therefore, advanced control systems incorporating knowledge of the plasma behavior provide extremely attractive options to improve device performance. Advances were made in stabilizing HFS and low-q plasmas in a controlled experiment environment through modeling-driven control schemes.

3.1. 3D magnetic equilibrium modeling

While 2D magnetic equilibria are well suited for equilibrium reconstruction in tokamaks, they cannot capture the behavior of 3D fields interacting with the main plasma. Therefore, these models are insufficient for proper reconstruction of the island divertor's magnetic geometry. Up to this point, J-TEXT's divertor field distributions were obtained by superimposing the RMP coil fields directly on top of the (plasma-driven) equilibrium magnetic fields. This approach is called the 'vacuum approximation', as it neglects the interaction between the main plasma and the RMP fields. Such an approach fails to consider screening effects from the main plasma, which produce a nonlinear response to the externally applied field.

The predictions from such a vacuum assumption model were refined by the incorporation of the full-field nonlinear resistive MHD model HINT [46, 47]. These calculations revealed local deviations in the current density around and inside the magnetic islands (see figure 2), which induced significant changes in the island size, position, and shape between full-field MHD and the vacuum assumption. The prediction of these deviations could in turn be backed up by experimental evidence from J-TEXT plasma discharges.

3.2. 3D plasma and impurity transport modeling

In order to leverage the full 3D knowledge of the magnetic configuration, the associated transport codes also need to be able to perform full 3D simulation. Due to the traditional focus on poloidal divertor operation, this is an area traditionally somewhat neglected in tokamak research (with a few exceptions, such as TEXTOR-DED), while being of extremely high relevance for stellarators.

For J-TEXT, the recent research in this area is focused on integrating the EMC3-EIRENE code package into tokamak simulation workflows. EMC3-EIRENE is a coupled code combining the 3D edge plasma fluid Monte Carlo code EMC3 with the impurity Monte Carlo model EIRENE. EMC3-EIRENE can operate in non-axisymmetric plasmas, making it a popular edge transport code for stellarators. As an initial benchmark application, EMC3-EIRENE was employed to investigate the relationship between the exact magnetic geometry of the divertor (particularly the X-point location) and the impurity distribution and radiation in the plasma edge (see figure 3 for an example). Comparisons with high-density experiments showed a reasonable agreement between

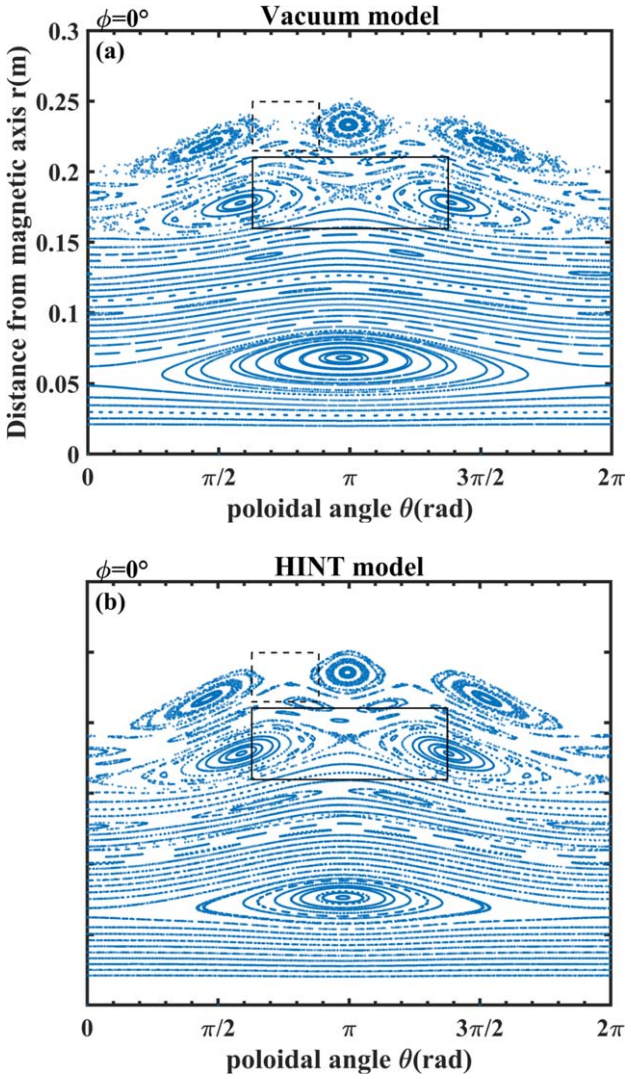

Figure 2. Poincaré plots of the vacuum approximation (2D MHD equilibrium + RMP) and HINT (3D MHD equilibrium) model at $\Phi = 0^\circ$ for $I_{\mathrm{RMP}} = 3$ kA. (a) Vacuum model, (b) HINT model. The solid rectangle marks an X-point of the $2/1$ magnetic island chain and the dashed rectangle marks an X-point of $3/1$ magnetic islands. Reprinted from [47], with the permission of AIP Publishing.

simulations and modeling, demonstrating the readiness of the code package (particularly concerning its strong requirements on grid generation) for tokamak divertor topologies [48].

Another important aspect of edge transport modeling is the assessment of heat loads onto the PFCs. Whereas axisymmetric configurations usually only produce a set of similarly symmetric strike-lines, the introduction of 3D fields into the magnetic geometry substantially complicates the resulting heat load patterns. While 3D edge transport codes such as EMC3-EIRENE are fully capable of producing heat load distributions on their domain boundaries, these codes are primarily designed to investigate the edge plasma volume. On the one hand, this imposes strict quality requirements on the grid generation process (which hinders automation and bulk analysis of many magnetic configurations), while, on the other hand, this also limits the expressiveness of the codes

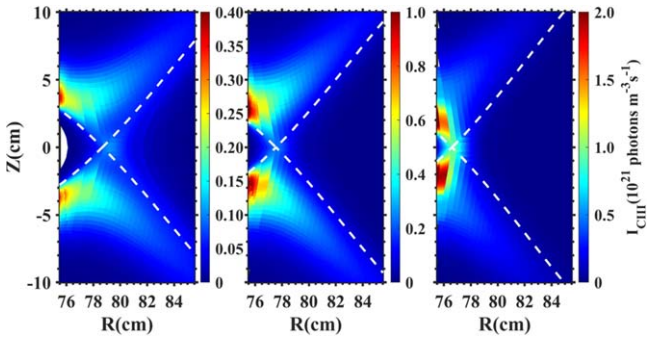

Figure 3. C III radiation intensity distributions simulated with EMC3-EIRENE at distinct divertor coil currents of 15, 12, and 10 kA. The dashed lines represent the locations of the separatrix. Reproduced from [48]. © 2021 Hefei Institutes of Physical Science, Chinese Academy of Sciences and IOP Publishing. All rights reserved.

regarding the exact PFC geometry (by restricting boundary meshes onto grid cell interfaces).

To remedy these issues, a purpose-built Monte Carlo proxy model was realized based on simple anisotropic diffusion (with parallel/perpendicular diffusion coefficient ratios of about 10^6–10^7) [49]. The linearity of this model implies that all test packets could be traced independently, eliminating the need for any sort of accumulation grid. By directly relying on high-resolution meshes for the boundary representation, this model could produce fine-grained predictions of heat load distributions. Recent investigations on the Wendelstein 7-X (W7-X) stellarator revealed the necessity of a diffusive parallel transport mechanism, as counter-streaming flows (which are rare in axisymmetric geometries) can have significant influence on the heat load distribution. After successful application on W7-X, this anisotropic diffusion model is currently in application on J-TEXT for the investigation of the island divertor configuration.

3.3. Accurate transport and PWI modeling for advanced divertor configurations

In addition to the investigation of 3D fields, efforts have also been made to improve the understanding and accurate plasma state reconstruction of advanced axisymmetric divertor scenarios. Modern divertor configurations such as Snowflake, Super-X, HFS divertors, or double-null configurations, are particularly substantially more sensitive to drift effects when compared to classical single-null poloidal divertors.

A code particularly suited for analyzing drift-sensitive edge transport scenarios is the SOLPS-ITER package. Like EMC3-EIRENE, SOLPS-ITER is a combination of dedicated models for the edge plasma transport and the impurity transport. However, instead of relying on EMC3, SOLPS-ITER instead uses the B2.5 plasma solver. B2.5 is a fast 2D transport solver for axisymmetric configurations, which features a particularly comprehensive physics model, including terms for main plasma drifts.

While the application of SOLPS-ITER to J-TEXT is actively underway (focusing in particular on the HFS poloidal

divertor scenarios), it was also employed to investigate experimental scenarios on the close-by EAST tokamak [50]. There, it was used to provide a detailed study relating the magnetic field direction with SOL density profiles and fall-off lengths, which made wide use of the code's comprehensive and detailed physics model.

3.4. Plasma instability modeling

One major obstacle to operation with a HFS divertor is the radial instability of the HFS middle-single-null configuration. In order to define and extend the operational window surrounding this instability, a filament-based force-balance model was developed to simulate the dynamic radial movement of the plasma in a feedback-controlled environment (where feedback was provided via the vertical field coils). Results from this indication showed that the HFS divertor configuration could be sufficiently stabilized for active feedback control by shifting the magnetic axis location slightly outward compared to standard operation [51].

The instability model was then expanded upon by incorporating the dynamic behavior of the feedback control system itself into the simulation. Through joint simulation of both the instability and the feedback control, the stability domain of the control scheme could be determined both in configuration space (axis position, plasma beta) and the feedback control parameters. This analysis revealed the optimal response parameters for the feedback control system, which allowed for more effective suppression of the radial instability and an extended operation space for the HFS divertor configuration [52].

The second focus of instability research was the investigation of low-q plasma stabilization through external 3D fields. In recent years, investigating the impact of 3D magnetic perturbations (MPs) on plasma stability has become a major focus of J-TEXT research. A major instability is the ideal kink mode, which usually imposes a lower boundary of $q_{\mathrm{edge}} \geqslant 2$ on tokamak operation. For J-TEXT, the behavior of these plasmas was investigated with the MIPS code. MIPS incorporates a nonlinear resistive 3D MHD model, which includes the effects of magnetic reconnection and nonlinearities due to pressure profile redistribution.

By analyzing the behavior of the kink mode in an external 3D field, it was found that a pair of opposite iota $= 1$ coils can be used to stabilize the kink mode and suppress its growth by adding a small background $m = 2$, $n = 2$ component to the edge magnetic field [53]. Such a coil pair might be used in the near future on J-TEXT to experimentally investigate the stabilization of the low-q regime.

3.5. Discussions and future challenges

The divertor configurations of J-TEXT present highly attractive targets to benchmark integrated edge modeling, particularly due to its combination of agile small-scale operation and the wide array of advanced magnetic configurations available. On this test bed, the individual components required for comprehensive edge modeling have shown promising benchmarking results and good capability to handle unusual magnetic configurations.

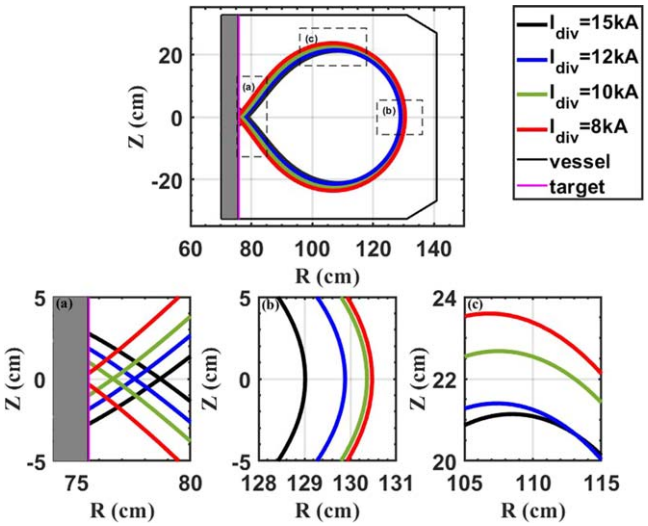

Figure 4. LCFS generated from the Equilibrium FITting code EFIT for the HFS-MSN divertor configurations with different divertor coil currents and enlarged views of three regions. Reproduced from [48].

The next step will now be to integrate all these 3D modeling workflows into a single unified analysis approach. This will require an efficient exchange of data between the individual codes and tight coordination between individual researchers, and care will have to be taken in how to achieve a consistent picture in the different models. However, thanks to the performed in-depth validation studies, this integration effort can now take place with a strong confidence in the individual codes themselves.

4. HFS poloidal divertor configuration

At the end of 2018, a special poloidal divertor configuration with a mid-plane single null at the high-field side (HFS-MSN) was successfully realized for the first time on J-TEXT by utilizing three sets of divertor coils (DV) and two sets of bias coils (BS). These DV and BS coils located in the inner cylinder were carried over from the previous TEXT-U tokamak. By tuning the amplitude and orientation of the current flowing in each of these coils, it is possible to flexibly change the divertor configuration from single-null (SN) to double-null (DN), as well as the X-point location, during the discharge. To maximize the heat load handling capability for the divertor plasma operation, a SiC-coated graphite divertor target fully covering the entire inner wall was newly constructed. To date, J-TEXT is the only device in the world capable of operating in various different HFS divertor configurations, especially with the HFS-MSN, where the X-point is located in the favorable-curvature area.

Compared with the limiter configuration, the HFS-MSN divertor configuration (an example is shown in figure 4) greatly increases the wetted area, and reduces the peak heat

flux on the target plate, which may mitigate the sputtering of impurities. In this section, recent approaches in various experiments, including the density limit, radiating divertor, and detachment on J-TEXT with the HFS-MSN divertor configuration will be highlighted. Furthermore, experiments investigating the impact of E_r on the up–down asymmetry of divertor loads (using the electrode biasing system) will be presented as well.

4.1. Density limit/X-location dependence

Recently, a series of high-density experiments in divertor configuration was carried out on J-TEXT [48]. An extension of the density limit from a Greenwald fraction of 0.79–0.85 was achieved by changing the ohmic plasma from the limiter configuration to the HFS-MSN configuration (as shown in figure 5). In this experiment, the plasma density was ramped up through gas puffing from the bottom flange. Due to the lack of wall conditioning between shots, the recycling of the wall in the shots of $I_{\rm div} = 10$ kA (#1070668) and $I_{\rm div} = 8$ kA (#1070669) is stronger after huge gas filling in the shots of $I_{\rm div} = 15$ kA (#1070665) and $I_{\rm div} = 12$ kA (#1070667). It causes the initial density to be very high. With the increasing plasma density, the SOL electron temperature dropped, and the downstream ion saturation flux increased faster than the upstream ion saturation flux, which may result from the radial transport changes with the density ramp-up. Meanwhile, the impurity radiation was enhanced, which is helpful in reducing the target heat load. However, under ohmic discharge conditions, the core radiation still dominates even in divertor plasmas, resulting in difficult access to further high-density operation domains.

Moving the X-point away from the divertor target was shown to improve the density limit, and to result in an increase in the peak divertor heat flux and a decrease in the divertor heat flux decay length. Constrained by an open divertor without a neutralizing gas pumping system and low heating power, the high recycling regime has not been observed in the HFS-MSN divertor plasma on J-TEXT. The ratio of the downstream flux to the upstream flux is still linear as the plasma density rises.

In future experiments, the introduction of electron cyclotron resonance heating (ECRH) could help to further increase the edge plasma density and improve the edge plasma and impurity transport. This might enable the device to explore higher plasma density ranges, which would also be of interest to the HFS divertor studies.

4.2. Impurity transport/X-location dependence

The SOL impurity screening effect has been observed in the J-TEXT plasma with the HFS-MSN divertor configuration, and it is more favorable when the X-point location is moving away from the target plate. A comparison of the temporal variation of radiation profiles from the density ramp-up discharges with various X-point locations is shown in figure 6. The results show that the radiation intensity in both the core

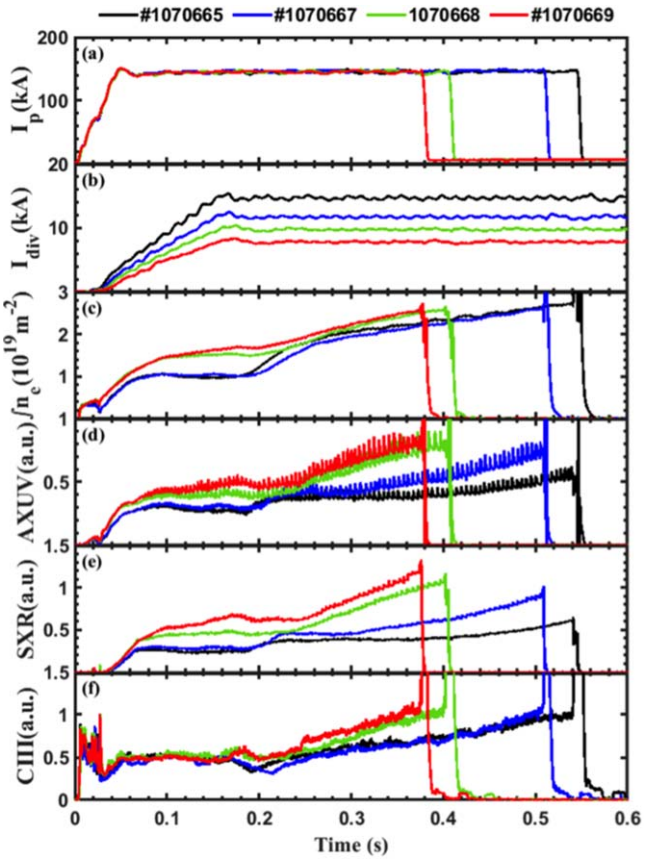

Figure 5. Time evolutions of the operation and plasma parameters with different DV currents. Reproduced from [48]. © 2021 Hefei Institutes of Physical Science, Chinese Academy of Sciences and IOP Publishing. All rights reserved.

and the SOL is reduced with the increasing divertor coil current $I_{\rm div}$ (which means the X-point moves away from the target).

In high-density HFS-MSN divertor plasma experiments, the density-normalized radiation intensity measured by Absolute eXtended UltraViolet (AXUV) and soft X-ray (SXR) diagnostics was reduced by more than 50% compared to that observed in the limiter configuration.

Doppler CIS provided 2D radiation signals to investigate the evolution of the C III radiation distribution near the HFS target before disruption. When comparing the signals at 200 ms and before disruption, the C III radiation distribution is concentrated to the HFS when the density increases, as shown in figure 7. Before disruption, the radiation intensity peaks with different $I_{\rm div}$ are near the same location. However, the location relative to the LCFS is deeper towards the core due to the X-point being closer to the target at low $I_{\rm div}$.

To better understand the underlying physics mechanisms, EMC3-EIRENE was applied to study the SOL plasma transport in HFS mid-plane single-null configurations on J-TEXT. Good qualitative agreements between the simulation results and experimental findings were obtained. The simulation results provided detailed 2D distributions of the main plasma parameters, as shown in figure 3.

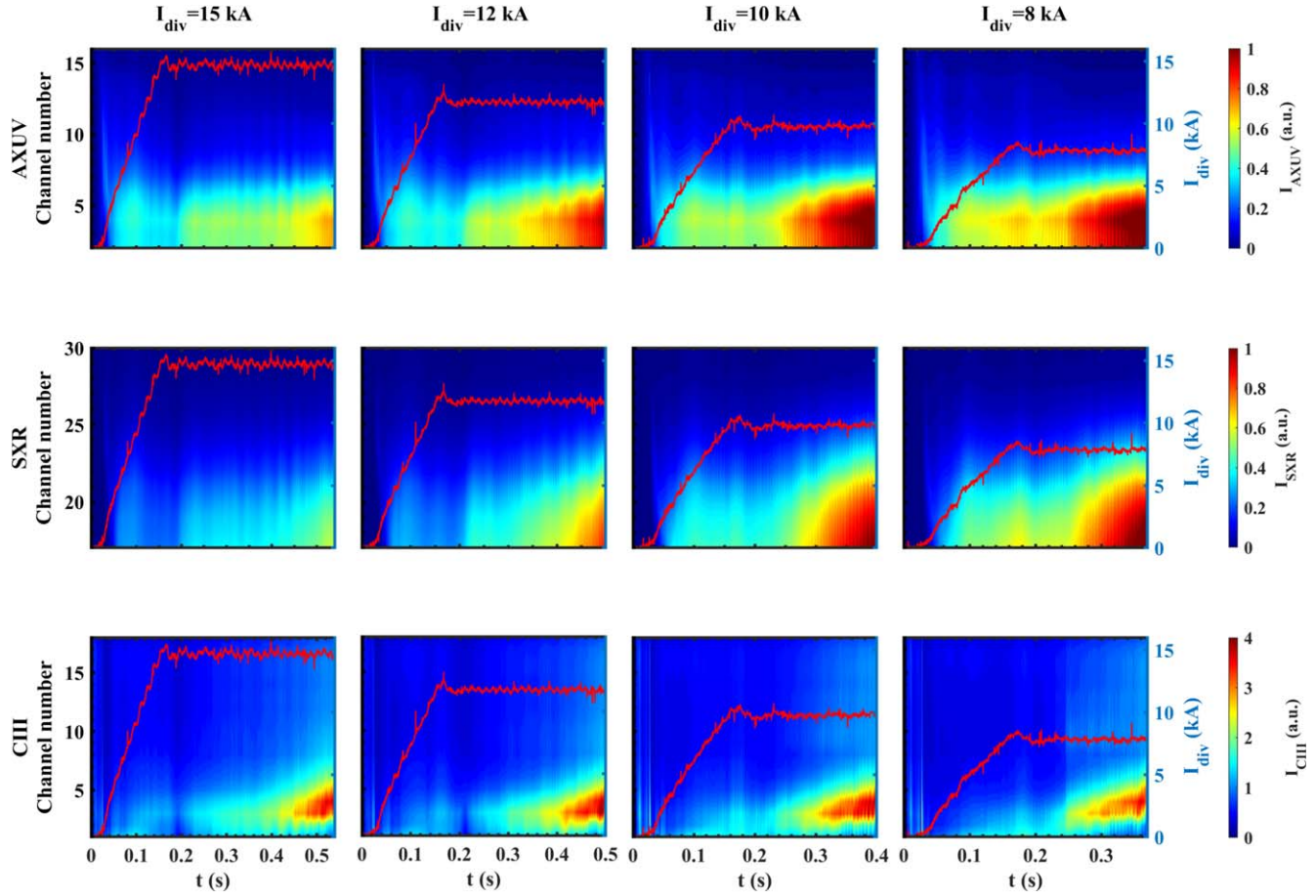

Figure 6. The waveforms of the AXUV, SXR, and C III signals. The red line is the DV current. Reproduced from [48]. © 2021 Hefei Institutes of Physical Science, Chinese Academy of Sciences and IOP Publishing. All rights reserved.

4.3. Radiative divertor

Radiative divertors, which dissipate plasma energy by actively controlling impurity radiation at the plasma boundary, have emerged as an attractive technology for reducing the heat load on the divertor plate and reaching detached plasmas in long-pulse high-performance plasma operation. Recent experimental efforts on the majority of existing tokamaks and stellarators have been made to exert finer control over detachment characteristics in order to optimize the reduction of heat flow to the divertor plates while simultaneously minimizing the influence of increased contamination and radiation on energy confinement.

The first experimental investigation of highly radiative divertor and detachment regimes with impurity gas seeding in the HFS-MSN divertor configuration was recently carried out on J-TEXT. Figure 8 shows an example discharge with methane (CH_4) seeding. In this experiment, stable HFS-MSN divertor configuration is formed from 0.2 s as the divertor current reaches its flat-top phase. The locations of the upper and lower strike points are around $Z_{tar} = \pm 3$ cm. A gas injection nozzle is embedded on the HFS divertor target plate in the mid-plane, and its location is just in the divertor private flux region. A high-pulse voltage waveform to control the piezoelectric crystal valve was preset at 0.3 s for injecting CH_4 (red line in figure 8(b)). After a delay of about 0.02 s (due to the gas tube length), it can be seen that the electron temperature, T_e, drops to around 5 eV and the heat flux, q_t, decreases near the strike points at $t = 0.32$ s (measured by divertor Langmuir probes). As shown in figure 8(f), the temporal evolution of the 2D C III radiation profiles with CH_4 gas puffing in the divertor region can be observed by a wide-angle visible light high-speed imaging system with a C III filter [41]. The preliminary results show that the C III radiation intensity at the lower strike point increases first, then the radiation at the upper strike point increases shortly after, and finally the radiation near the X-point also increases. With a continuous injection of CH_4, the divertor ion saturation current in the far SOL region (around $Z_{tar} = \pm 4.5$ cm) continued to increase, as shown in figure 8(d). The plasma line-averaged density also increased at the same time, and eventually led to a density limit disruption.

4.4. Impact of E_r on the up–down asymmetry of divertor loads

The in–out asymmetries of the heat flux and particle flux on the divertor target are key issues for future high-power long-pulse scenarios. The asymmetry arises from many factors, mainly including classical drifts (electric and diamagnetic drifts) [54, 55], ballooning instabilities, and Pfirsch–Schlüter flows [56]. So far, the electric drift $E_r \times B$ has been considered as a primary reason for the in–out asymmetry. Similar

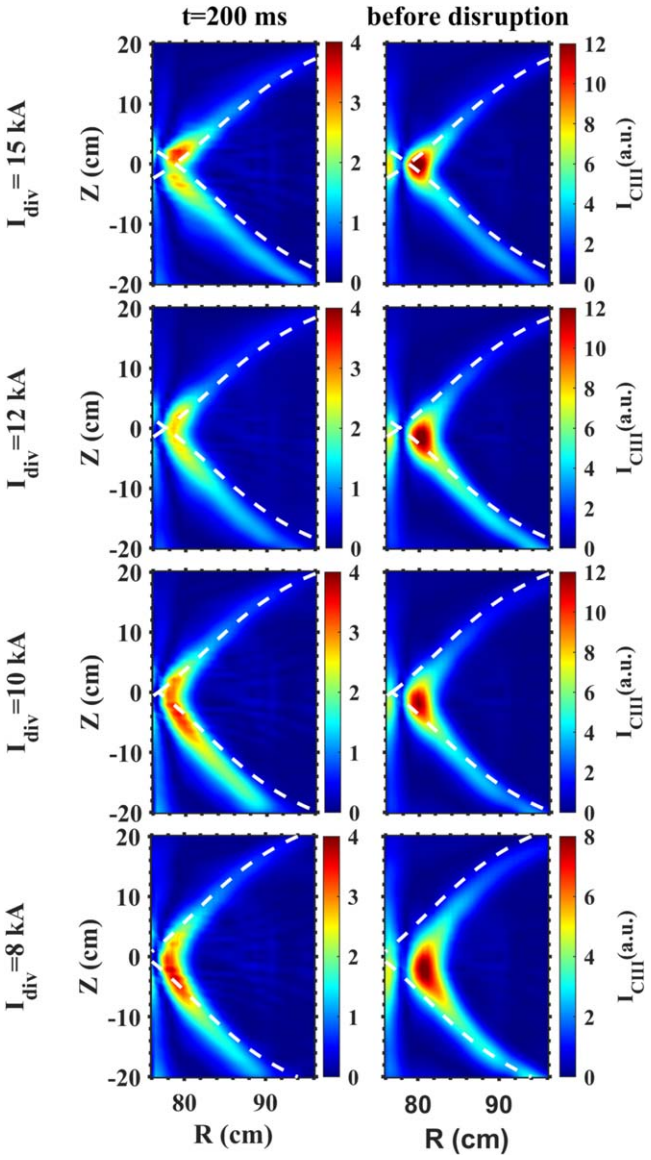

Figure 7. The radiation intensity distribution from CIS. The dashed white line is the separatrix. Reproduced from [48]. © 2021 Hefei Institutes of Physical Science, Chinese Academy of Sciences and IOP Publishing. All rights reserved.

to the in–out asymmetry, an obvious up–down asymmetry has been observed in the HFS-MSN divertor configuration on J-TEXT. In this experiment, the effect of the $E_r \times B$ drift on the up–down asymmetry was investigated, using a movable electrode bias (EB) to modulate the edge E_r.

The discharge parameters are as follows: the toroidal magnetic field $B_t = 2$ T, the plasma current $I_p = 120$ kA, the divertor coil current $I_{div} = 14$ kA, the central line-averaged density $n_e = 4 \times 10^{19}$ m^{-3}, and the radial position of the EB is at $r = 210$ mm (part of the EB enters the LCFS). As shown in figure 9(a), the orientation of the biasing voltage can significantly influence the radial field profile. Measurements of the ion saturation current profile (figure 9(c)) indicate a significant asymmetry in the particle fluxes, which is directly related to the applied bias voltage. A similarly significant response to the biasing application can be seen in the vertical distribution of the H_α radiation intensity measured by a PDA viewing the HFS (figure 9(d)). Without biasing, both I_s and H_α radiations at the upper strike point are stronger than those at the lower strike point. Under a positive biasing voltage of +300 V, the V_f (figure 9(b)) of the strike point increases, which indicates that the EB probe has touched the LCFS. The E_r in the SOL points outward and the amplitude increases significantly, so the direction of $E_r \times B$ drift points towards the upper strike point. This results in an increase in the asymmetry of the upper and down strike points. With a negative bias, the phenomenon is opposite to the positive case. In this case, the observed I_s and H_α radiations at the down strike point are higher than those at the upper strike point, and the asymmetry is reversed.

4.5. Future plans

Concerning the HFS divertor configuration on J-TEXT, the plasma parameter distribution near the divertor target plate and the radiation level near the X-point will be the near-time focus of later experiments. The combination of the X-point and the thermal instability, such as multifaceted asymmetric radiation from the edge (MARFEs) [12], on the HFS boundary will be further investigated to develop detachment scenarios and associated feedback control technology, aiming to reduce the negative impact of detachment on the plasma confinement and stability of the core. In addition, the existing electrode biasing system will be upgraded, and a biased divertor target will be constructed. After that, experiments with an actively controlled boundary electric field will be carried out to study the effect of $E \times B$ drift on the power decay length, detachment, and asymmetric heat flow of the upper and lower (inner and outer) target plates. Finally, an electrostatic control scheme will be proposed to control the heat load on the divertor target plate.

5. Island divertor configuration

The island divertor, one of multiple attractive advanced divertor concepts, has been successfully applied on the W7-AS stellarator, and further developed on the W7-X stellarator. In the island divertor configuration, the SOL is formed by a group of magnetic islands, which form closed flux tubes around the core plasma. These edge islands are then intersected and cut open by divertor target plates. Compared with the standard poloidal divertor configuration, the island divertor configuration has a weaker correlation with the plasma current and a longer connection length, which results in a wider distribution of heat loads and also makes it easier to enter stable detachment of divertor operation [57]. Therefore, it is of great interest and significance to apply and explore the island divertor configuration in tokamak plasmas. Recently, a first attempt has been made to form an island divertor configuration in the J-TEXT tokamak. In this section, the characteristics of this J-TEXT island divertor will be presented.

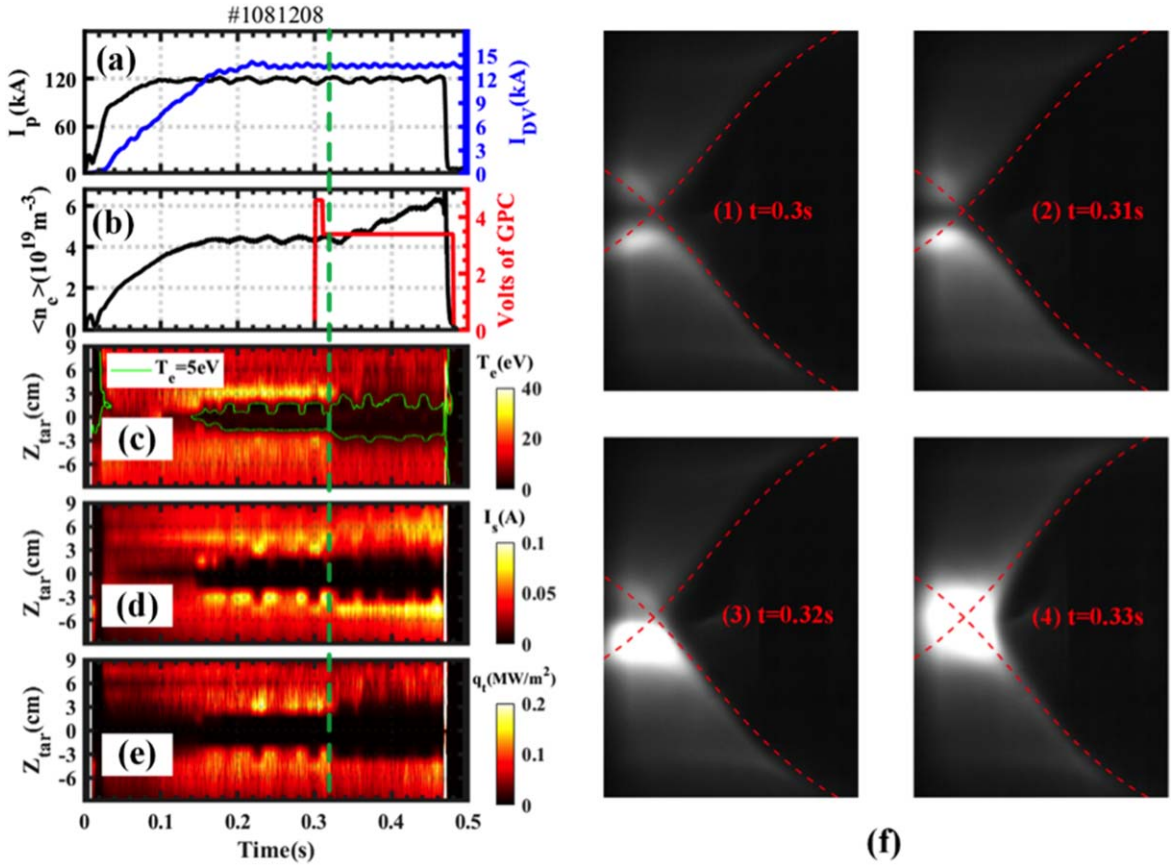

Figure 8. Plasma parameters for a high-density discharge (#1081208) with CH_4 seeding, (a) plasma current I_p (black) and divertor coil current I_{DV} (blue), (b) line-averaged density n_e (blue) and control voltage signal of HFS gas puffing (red), (c) divertor target plate electron temperature, T_e, (d) ion saturation current, I_s, and (e) heat flux, q_t, measured by divertor Langmuir probes, (f) visible imaging with C III filter, $t = 0.3$ s before CH_4 seeding, and $t = 0.31$ s, 0.32 s, 0.33 s after CH_4 seeding.

5.1. Formation of island divertor configuration

On J-TEXT, the first island divertor configuration was formed by moving the $m/n = 3/1$ edge island chain outward to intersect with the divertor target. Here, m and n are the poloidal and toroidal mode numbers, respectively. In this experiment, the $m/n = 3/1$ edge magnetic islands were excited by applying RMPs with a dominant $m/n = 3/1$ component [58, 59] in a limiter plasma with an edge safety factor, q_a, slightly over 3. By increasing the plasma current to reduce the edge safety factor, the edge magnetic islands are cut by the divertor target to finally build up the island divertor configuration. An example showing the formation of an island divertor configuration is presented in figure 10. When the $3/1$ edge islands are gradually opened by the divertor target ($t = 0.26$–0.4 s), the main striking points, indicated by the floating potential measurements (figure 10(g)) from the divertor Langmuir probe arrays, move to two sides ($R < 1.05$ m and $R > 1.05$ m) of the divertor target. This reveals that topological differences considerably affect the divertor heat load patterns. Once the $3/1$ edge islands are fully moved behind the divertor target, the island divertor configuration is then transformed back to a limiter configuration ($t > 0.4$ s). The formation of the island divertor configuration strongly depends on the edge magnetic topologies, or more specifically, the interactions

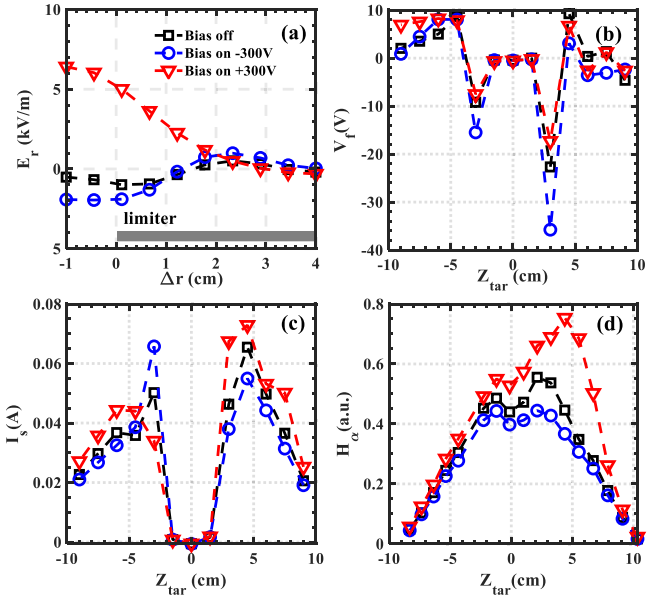

Figure 9. (a) Radial profiles of the radial electric fields E_r measured by reciprocating Langmuir probes; positive value means that the E_r points radially outward. (b) and (c) floating potential V_f and ion saturation current I_s distribution measured by the Langmuir probe array on the HFS divertor plate. (d) Vertical distribution of the H_α radiation intensity measured by PDA viewing the HFS.

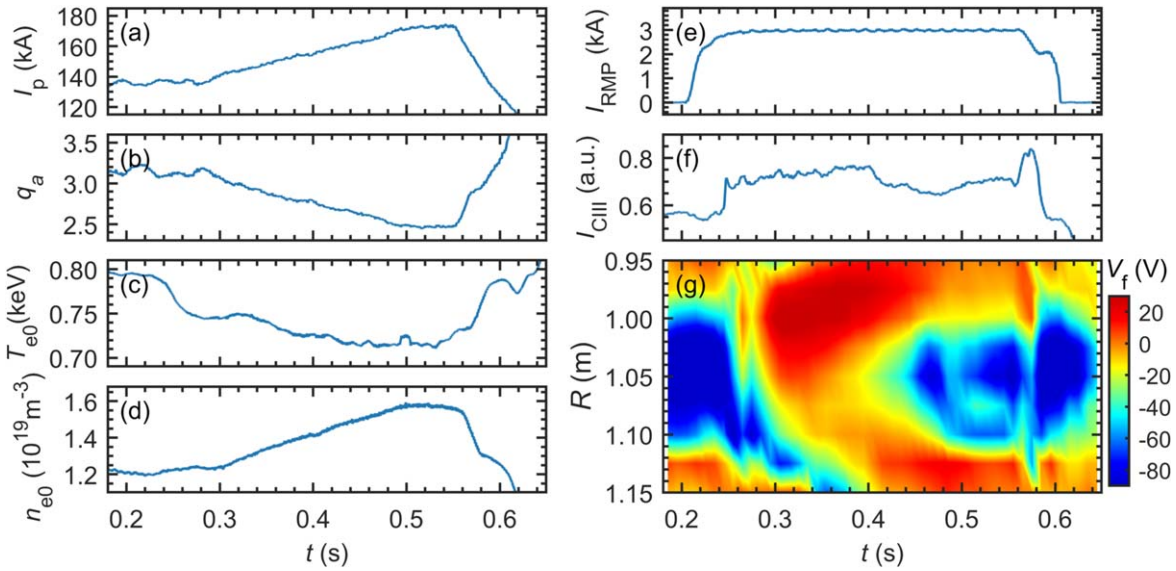

Figure 10. Overview of main plasma parameters for the experiment discharge #1056902 on J-TEXT, including (a) the plasma current, (b) the edge safety factor, (c) the electron temperature, (d) the electron density, (e) the RMP coil current, (f) the C III intensity near the plasma boundary, (g) the contour of the floating potential measured by the divertor Langmuir probes.

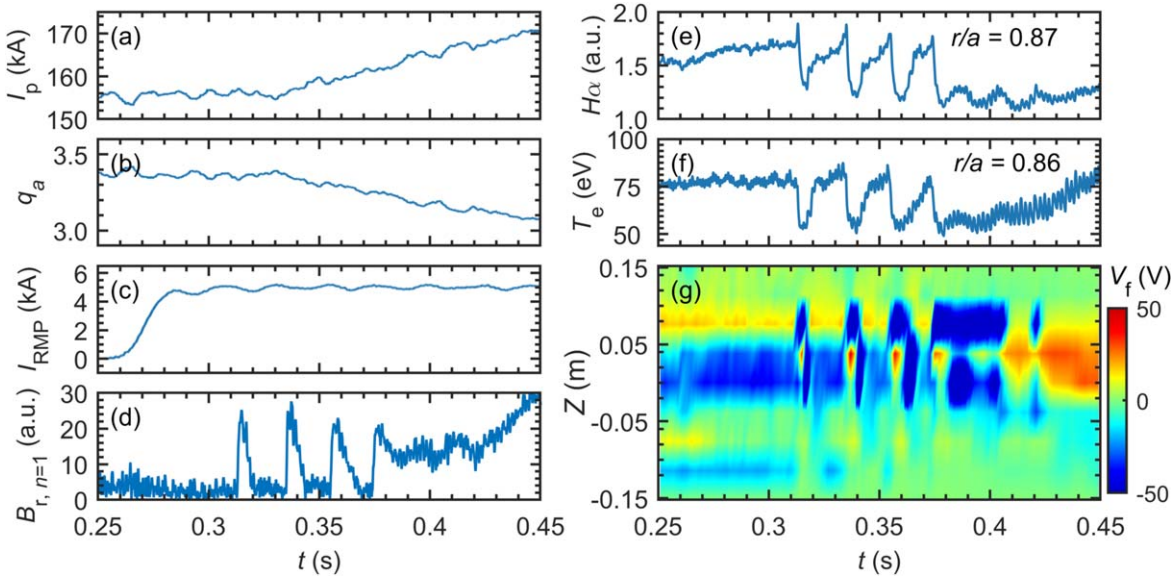

Figure 11. Overview of main plasma parameters for experiment discharge #1077700 on J-TEXT, including (a) the plasma current, (b) the edge safety factor, (c) the RMP coil current, (d) the radial magnetic field for the $n = 1$ part, (e) the H_α intensity, (f) the electron temperature, and (g) the contour of the floating potential measured by the divertor Langmuir probes.

between the edge island and the divertor target. By optimizing the edge magnetic topology and the structure of the target plate, the divertor heat load distribution could be significantly modified, so as to increase the power deposition area and reduce the peak heat load. Such optimization processes are being carried out on J-TEXT, leveraging both 3D edge transport modeling and dedicated experiments.

5.2. Stability of edge island

The operation of the island divertor configuration is closely tied to the stability of the edge island. Once there is a change in the width and phase of the edge island, the island divertor configuration cannot operate stably, which can even lead to the deposition of heat load outside the divertor targets. Therefore, the stability of the edge island is of great concern in the experiment. A new type of edge island instability, the so-called self-sustained divertor oscillation, was observed in J-TEXT (as shown in figure 11) during divertor experiments. Since a bifurcative oscillation of ~50 Hz is observed among the edge island width, the edge H_α intensity, and the edge electron temperature, the oscillation is regarded to be a sequential repetition of the magnetic field penetration-screening transition and back-transition. The periodic

collapses repeat several times until the edge islands are intersected by the divertor target (corresponds to $q_a = 3.1$). As the edge islands are gradually opened, the amplitude of the oscillation decreases, and the properties of the oscillation also change from burst-like ($t = 0.31$–0.38 s) to quasi-continuous ($t = 0.38$–0.42 s). Thus, the divertor target structure is also significant for the stability of the edge island. In addition, the divertor oscillation shows a correlated dependence on the plasma edge density. The detailed analyses and explanations are still to be investigated.

5.3. Impurity screening effects

The impurity accumulation at the central plasma is one of the burning issues for high-performance long-pulse plasma operation. Impurity control has become the focus of extensive attention in J-TEXT. During the application of the island divertor configuration, it was found that the $m/n = 3/1$ edge island has an impurity screening effect, especially when the O-point of the island is near the LFS divertor target. By combining a methane injection experimental study and STRAHL [60] impurity transport analysis, it was demonstrated that the variation of the impurity transport dominates the impurity screening effect. The impurity diffusion is enhanced with a significant increase in the outward convection velocity at the edge region [61]. The interactions of the edge island and the divertor target contribute to the impurity screening effects with the dependence on the edge island width and phase. Therefore, a better impurity exhaust/screening could also be achieved by optimizing the edge magnetic topologies. In addition, the radial electric field, the plasma rotation, and turbulence are considered to play an important role in impurity screening. The detailed impurity behaviors under the island divertor configuration will be studied with the foreseen application of 3D transport codes, such as EMC3-EIRENE. Moreover, combining the electric field, plasma rotation, and turbulence into integrated scenario modeling is another important topic for further studies.

5.4. 3D divertor heat loads

For the island divertor configuration, longer field-line connection lengths at the SOL (in the magnitude of 10^2–10^3 m, much longer than the electron mean free path) could be obtained, which benefits heat load spreading on the divertor target [62]. In order to investigate the effects of the edge magnetic topology on the divertor heat load distribution, a 2D infrared thermography camera system viewing the HFS divertor target from the LFS mid-plane window with a high spectral resolution of 0.5 mm was established on J-TEXT. During the experiments in island divertor configuration, the surface temperature distributions on the divertor target could be obtained in real time. It was demonstrated that the divertor surface temperature distributions could be modified with the change in the edge magnetic topology. However, the leading edges on the existing divertor target seriously affect the measurement of the heat load. Thus, a new set of divertor target plates should be designed and constructed. Currently, an analysis program for extrapolating the divertor heat load distribution from the divertor surface temperature is under development. Additionally, the heat exhaust capabilities of the island divertor configuration will be investigated in future campaigns.

5.5. Discussions and future challenges

The investigation of edge plasma physics relies heavily on appropriate diagnostics at the plasma boundary. In particular, in the tokamak equilibrium magnetic field configuration, the width of the edge island is generally narrow ($w = 1$–3 cm) due to the large magnetic shear, and therefore a high spatial resolution of the boundary diagnostics is greatly appreciated. In addition, owing to the 3D asymmetry of the island divertor configuration, measurements of edge plasma parameters need to be performed simultaneously at multiple (different poloidal and toroidal) locations during the experiment. Accordingly, the boundary diagnostics on J-TEXT are being gradually optimized and improved.

The key points of the island divertor research on J-TEXT are to demonstrate its performances of heat and particle exhaust. Moreover, it is worthwhile to explore how to realize stable detachment operation of the island divertor, which may rely on the synergy effects of the optimized magnetic topology, plasma transport, and heat load dissipation (through impurity seeding). In particular, the core–edge integration to develop and demonstrate dissipative/detached divertor solutions for power and particle control, sufficient for extrapolation to high-performance long-pulse H-mode plasma conditions, is worth investigating.

6. Other new divertor concepts

The toroidal symmetric poloidal divertor configuration is usually modified to a 3D boundary by applying RMPs for the purpose of controlling ELMs [24, 63]. The RMP fields for ELM control are generally produced by in-vessel saddle coils, which may face great challenges in a future reactor, and have clear q_{95} windows. Therefore, new approaches for generating RMP fields have to be proposed or tested. The non-axisymmetric (NA) helical currents induced by lower hybrid waves in the SOL were observed to impact the magnetic topology profoundly and to strongly mitigate ELMs in EAST [24]. ELM control using NA-SOL currents induced by the NA biased divertor plates has been proposed; the RMP field driven by this technique has been evaluated for ITER, and the predicted currents are sufficient to control ELMs in ITER [63].

These promising results motivate the experiments carried out on J-TEXT [64–66], which aim at verifying the ability of edge biasing-driven NA-SOL currents to modify the boundary magnetic topology. The basic concept is to utilize the movable electrode to apply a local biasing in the SOL of the J-TEXT plasma. Then the currents can be induced helically along the flux tubes towards the limiter or divertor plates, as illustrated in figure 12.

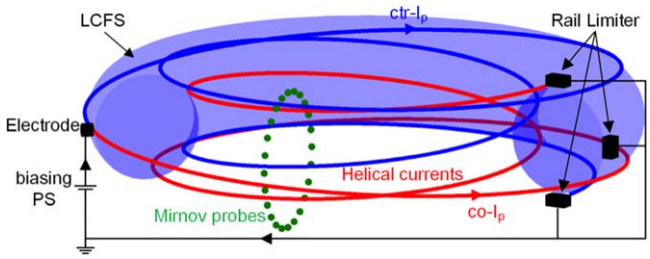

Figure 12. Schematic diagram of the SOL current driven by the biased electrode in the limiter plasma of J-TEXT.

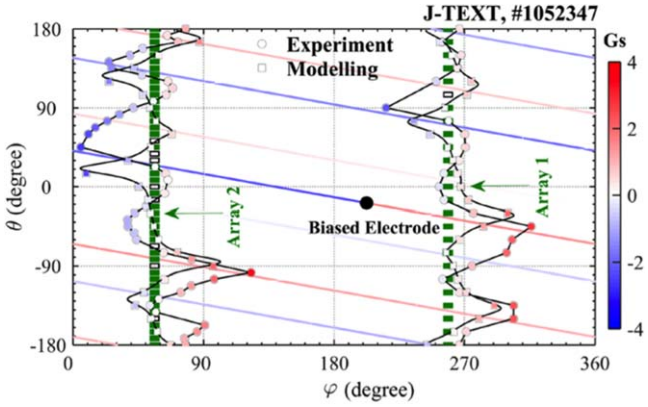

Figure 13. The comparison between measured δB_θ (circles) and modeled δB_θ (squares), showing the toroidal non-axisymmetric feature of the MPs generated by the biasing-induced SOL currents. Reproduced courtesy of IAEA. Figure from [64]. Copyright 2019 IAEA.

As a first step, the experiments were carried out in the limiter configuration to study the basic features of the biasing-driven SOL currents [64, 65]. By applying a modulated voltage to the electrode, the electrode current is modulated at the same frequency. Using the poloidal Mirnov probe arrays located at two toroidal angles, the poloidal magnetic field is also measured to be modulated at the same frequency, and the amplitude (δB_θ) is shown in figure 13 with the total electrode current being 150 A. Clear peaks and valleys can be identified from the poloidal distribution of δB_θ; in particular, the peaks are located at different poloidal locations for the two arrays, indicating the toroidal NA feature of the MPs. The squares in figure 13 represent the calculated δB_θ obtained from a model with helical currents flowing in either direction in the flux tube of the electrode and decaying to zero after a full poloidal turn. Most of the experimental features are captured by this simple model, proving that the biased electrode can induce helical current in the SOL and produce NA MPs.

Further development of the model for biasing-induced SOL currents improves the description and understanding of the experimental data [65–67]. On one hand, by replacing the straight field line assumption with the toroidal geometry, the peaks/valleys of the modeled δB_θ lie exactly at the experimental ones [65]. Treating the electrode with finite size provides various flux tubes, which then connect to various

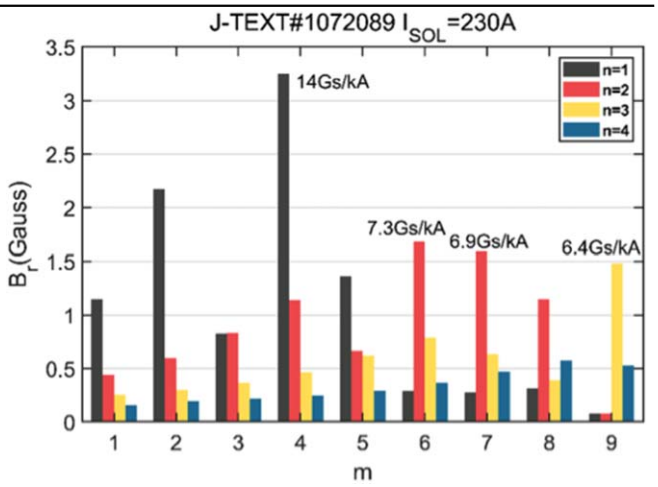

Figure 14. Radial magnetic field components obtained by the model on the q_{95} surface generated by the SOL current. Reproduced from [66]. © IOP Publishing Ltd. All rights reserved.

limiters, and more reasonable currents collected by the limiters can be calculated. On the other hand, using particle-in-cell simulations with a simplified 2D geometry provides a physical understanding of the decay of the SOL current along the flux tube, i.e. the linear decay electron current is balanced by the ion cross-field currents [67].

The SOL currents were then induced by electrode biasing in a poloidal divertor configuration on J-TEXT [66]. The NA feature of the corresponding MPs is also identified by the measurement from the magnetic probe arrays. The modeling result shows that MPs with an amplitude of 14 G/kA for the 4/1 component can be induced on the q_{95} surface (figure 14). More importantly, the impact of NA-SOL currents on the boundary magnetic topology has been observed by the tangential visible CCD camera, as shown in figure 15. Figure 15(a) displays the modeled Poincaré plot near the X-point, where a clear lobe structure is observed above the upper divertor leg, striking the target at $Z \approx 0.04$ m. In the photo shown in figure 15(b), the blue arrow indicates the upper divertor leg (or upper strike line) while the white arrow indicates the appearance of the lobe structure. This is clear evidence that the boundary magnetic topology can be modified by the NA-SOL currents induced via biasing. It is noted that the modeled Poincaré plot with the experimental SOL current (265 A) shows a shorter lobe structure (see figure 11(a) in reference [66]) compared to that shown in figure 15(a), which has a two times larger I_{SOL} (795 A) for better comparison. A more accurate comparison to the experimental picture requires the consideration of the plasma response to I_{SOL} and the synthetic diagnostic in the modeling, which will be left for future study. Since the current J-TEXT experiments use only a small electrode, the maximal amplitude of the NA-SOL current is limited. Future experimental attempts with asymmetric divertor biasing [63] are attractive, and HL-2A seems to be prepared for the following challenge [68].

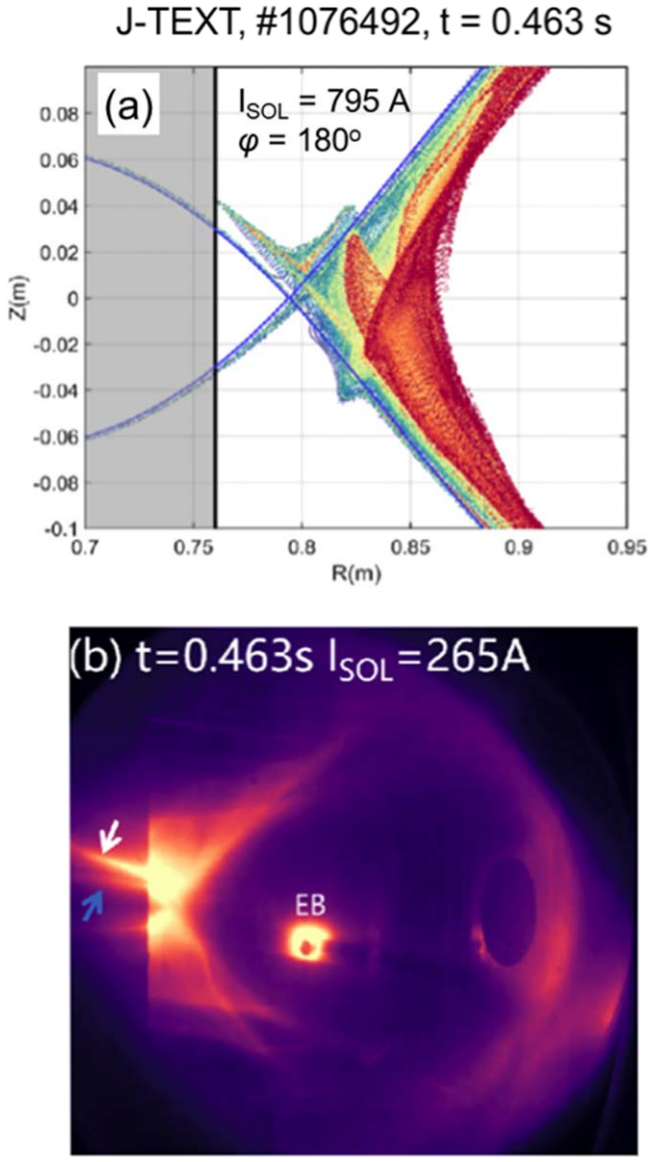

Figure 15. Impact of NA-SOL currents on the boundary magnetic topology in the poloidal divertor configuration. Reproduced from [66]. © IOP Publishing Ltd. All rights reserved.

7. Summary

In summary, to support the study of advanced divertor configurations and their associated fundamental edge divertor plasma physics, the J-TEXT team has devoted a considerable effort not only to the design of various new divertor configurations, but also to the development of edge plasma diagnostics and integrated modeling. Several important milestones have been achieved on J-TEXT in the last few years, including:

- First realization of the HFS-SN poloidal divertor plasma.
- Successful demonstration of using saddle coils to form island divertor plasmas in a tokamak device.
- First-time use of bias electrodes to drive and actively control SOL current filaments to form 3D plasma boundaries.

Preliminary explorations of fundamental divertor plasma physics such as impurity screening/transport, density limit, up–down asymmetry of divertor loads, radiative divertor, and detachment have been carried out on J-TEXT with these new divertor configurations. While the first experimental results are encouraging and interesting, further systematic studies and comparison with modeling results, especially on the synergy between 3D edge physics and PWIs, are still ongoing.

Due to their limited heating capability, J-TEXT plasmas currently operate in the low-confinement regime (L-mode). To extend the plasma operation domain and explore the coupling between new divertor configurations and high-performance core plasma, further upgrades of the ECRH heating system and the development of a new wall conditioning technology have been planned on J-TEXT.

Acknowledgments

This work is supported by the National MCF Energy R&D Program of China (Nos. 2018YFE0309100 and 2018YFE0310300), the National Key R&D Program of China (No. 2017YFE0302000), and National Natural Science Foundation of China (No. 51821005).

ORCID iDs

Yunfeng LIANG (梁云峰) https://orcid.org/0000-0002-9483-6911
Zhifeng CHENG (程芝峰) https://orcid.org/0000-0001-6019-399X
Philipp DREWS https://orcid.org/0000-0002-6567-1601

References

[1] Fujiwara M *et al* 2001 *Nucl. Fusion* **41** 1355
[2] Wan B N *et al* 2019 *Nucl. Fusion* **59** 112003
[3] Park H K *et al* 2019 *Nucl. Fusion* **59** 112020
[4] Klinger T *et al* 2019 *Nucl. Fusion* **59** 112004
[5] Bucalossi J *et al* 2022 *Nucl. Fusion* **62** 042007
[6] Wolf R C *et al* 2019 *Phys. Plasmas* **26** 082504
[7] Pitcher C S and Stangeby P C 1997 *Plasma Phys. Control. Fusion* **39** 779
[8] Eich T *et al* 2011 *Phys. Rev. Lett.* **107** 215001
[9] Kobayashi M *et al* 2013 *Nucl. Fusion* **53** 093032
[10] Feng Y *et al* 2005 *Nucl. Fusion* **45** 89
[11] Finken K H *et al* 1999 *Nucl. Fusion* **39** 637
[12] Liang Y *et al* 2005 *Phys. Rev. Lett.* **94** 105003
[13] Wang L *et al* 2021 *Nat. Commun.* **12** 1365
[14] Ohyabu N *et al* 1994 *Nucl. Fusion* **34** 387
[15] Feng Y *et al* 2021 *Nucl. Fusion* **61** 086012
[16] Bader A *et al* 2017 *Phys. Plasmas* **24** 032506
[17] Labit B *et al* 2017 *Nucl. Mater. Energy* **12** 1015
[18] Kolemen E *et al* 2018 *Nucl. Fusion* **58** 066007
[19] Zhang C *et al* 2020 *Fusion Eng. Des.* **158** 111678
[20] Katramados I *et al* 2011 *Fusion Eng. Des.* **86** 1595
[21] Evans T E *et al* 2004 *Phys. Rev. Lett.* **92** 235003
[22] Liang Y *et al* 2007 *Phys. Rev. Lett.* **98** 265004
[23] Liang Y *et al* 2010 *Phys. Rev. Lett.* **105** 065001

[24] Liang Y *et al* 2013 *Phys. Rev. Lett.* **110** 235002
[25] Liang Y *et al* 2010 *Nucl. Fusion* **50** 025013
[26] Liang Y *et al* 2013 *Nucl. Fusion* **53** 073036
[27] Zheng G Y *et al* 2012 *Chin. Phys. Lett.* **29** 105202
[28] Maddaluno G *et al* 2017 *Fusion Eng. Des.* **122** 341
[29] Liang Y *et al* 2019 *Nucl. Fusion* **59** 112016
[30] Edmonds P H *et al* 1988 The design of an inner poloidal divertor for the text tokamak ed A M van Ingen *et al Fusion Technology 1988* (Amsterdam: Elsevier) 342
[31] Ding Y H *et al* 2018 *Plasma Sci. Technol.* **20** 125101
[32] Zhang X B *et al* 2022 *Plasma Sci. Technol.* **24** 064007
[33] Wang N C *et al* 2022 *Nucl. Fusion* **62** 042016
[34] Wan Y X *et al* 2017 *Nucl. Fusion* **57** 102009
[35] Chen Z P *et al* 2012 *Plasma Sci. Technol.* **14** 1041
[36] Li F M *et al* 2016 *Rev. Sci. Instrum.* **87** 11D436
[37] Yang Q H *et al* 2022 *Plasma Sci. Technol.* **24** 054005
[38] Liu H *et al* 2016 *Plasma Sci. Technol.* **18** 601
[39] Liu H *et al* 2016 *Rev. Sci. Instrum.* **87** 11D444
[40] Yang J *et al* 2019 *Plasma Sci. Technol.* **21** 105105
[41] Xia M H *et al* 2019 *Fusion Eng. Des.* **146** 578
[42] Cheng Z F *et al* 2013 *Rev. Sci. Instrum.* **84** 073508
[43] Cheng Z F *et al* 2014 *Rev. Sci. Instrum.* **85** 11E423
[44] Zhang X L *et al* 2019 *Fusion Eng. Des.* **147** 111241
[45] Li B L *et al* 2022 *Fusion Eng. Des.* **184** 113271
[46] Suzuki Y 2017 *Plasma Phys. Control. Fusion* **59** 054008
[47] Wang Z S *et al* 2021 *Plasma Sci. Technol.* **23** 085104
[48] Wang H *et al* 2021 *Plasma Sci. Technol.* **23** 125103
[49] Knieps A *et al* 2022 *Plasma Phys. Control. Fusion* **64** 084001
[50] Wang F *et al* 2022 *Nucl. Fusion* **62** 056021
[51] Xu X *et al* 2022 *Phys. Plasmas* **29** 032510
[52] Han C *et al* 2022 *Fusion Eng. Des.* **178** 113099
[53] Huang J, Suzuki Y and J-TEXT Team 2021 *Plasma Fusion Res.* **16** 2403047
[54] Du H L *et al* 2016 *Plasma Phys. Control. Fusion* **58** 085006
[55] Rozhansky V *et al* 2012 *Nucl. Fusion* **52** 103017
[56] Asakura N *et al* 2004 *Nucl. Fusion* **44** 503
[57] Jakubowski M *et al* 2021 *Nucl. Fusion* **61** 106003
[58] Rao B *et al* 2014 *Fusion Eng. Des.* **89** 378
[59] Zhou S *et al* 2019 *Fusion Eng. Des.* **146** 902
[60] Behringer K 1987 Description of the impurity transport code STRAHL Technical Report JET-R (87)08 Abingdon: JET Joint Undertaking
[61] Zhang X L *et al* 2021 *Plasma Sci. Technol.* **23** 125101
[62] Zhou S *et al* 2022 *Nucl. Fusion* **62** 106002
[63] Joseph I, Cohen R H and Ryutov D D 2009 *Phys. Plasmas* **16** 052510
[64] Wang N C *et al* 2019 *Nucl. Fusion* **59** 096047
[65] Li S H *et al* 2021 *Plasma Phys. Control. Fusion* **63** 115017
[66] Li S H *et al* 2022 *Plasma Phys. Control. Fusion* **64** 075005
[67] Zhang H X *et al* 2020 *Plasma Sci. Technol.* **22** 105102
[68] Cui B T *et al* 2021 *Fusion Eng. Des.* **173** 112963